International Journal of Material and Mechanical Engineering, 2012, 1: 44-49
Published Online April 2012

www.ijm-me.org

Structural, electric and magnetic properties of $PrSrCoO_4$ and $Pr_{0.4}Sr_{1.6}CoO_4$ layered perovskites

A. Hassen
Department of Physics, Faculty of Science, Fayoum University, 63514 El Fayoum, Egypt
Department of Physics, Faculty of Science and Education, Taif University, KSA
Email: arafahassen@yahoo.com and ash02@fayoum.edu.eg

(**Abstract**) The structural, electric and magnetic properties of $PrSrCoO_4$ and $Pr_{0.4}Sr_{1.6}CoO_4$ layered perovskites have been investigated. The Rietveld refinements of x-ray powder diffraction (XRD) patterns at room temperature indicate that the samples crystallize in K_2NiF_4-type structure with group symmetry I4/mmm. The specimens exhibit semi-conducting behavior. The electric mechanism of $PrSrCoO_4$ obeys Arrhenius law and might be understood by small polaron models. On the other hand, the conduction of $Pr_{0.4}Sr_{1.6}CoO_4$ follows two-dimensional variable range hopping model (2D-VRH). The magnetic properties of $PrSrCoO_4$ show Curie-Weiss paramagnetic behavior within the studied range of temperature. While $Pr_{0.4}Sr_{1.6}CoO_4$ exhibits two magnetic transitions; one is due to Griffiths phase and second because of a mixture between ferromagnetic (FM) and antiferromagnetic (AFM) transitions. These transitions become broad and shifted towards low temperatures with increasing applied field. No complete FM state was observed for this higher content of Sr. Comparison with similar compounds of the same Sr content is also discussed models.

Keywords: layered perovskites , electric resistivity, semiconductors, magnetic measurements

1. INTRODUCTION

Cobalt oxides have particular interest, not only because of the unique features of Co ions, but also due to their technological applications, such as solid oxide fuel cells and membranes for gas separation.[1–5]. Moreover, perovskite cobaltates exhibit rich magnetic properties including different types of ordering phenomena such as paramagnetic (PM), antiferromagnetic (AFM), or ferromagnetic (FM). Double exchange interaction between $Co^{+3} - O - Co^{+4}$ is known to be FM while super-exchange interaction between Co ions with the same oxidation of states is AFM [6–9] The crystal-field splitting energy of Co *d*-states (E_{cf}) and Hund energy (E_{ex}) are comparable for perovskite cobaltates. This means that the energy gap between the t_{2g} and e_g states is small and the electrons in t_{2g} can be thermally exited into the e_g state. As a result high spin states can be archived [10]. In addition, the differences in electric or magnetic properties of cobaltates can be understood by considering the relationship between the average ionic radius of $R_{1-x}A_x$ (R is the rare earth ions and A is the alkalic ions) and the energy difference between the low spin and intermediate spin states.

Similar to isotropic perovskite compounds $R_{1-x}Sr_xCoO3$, the physical properties of layered perovskite system $R_{2-x}Sr_xCoO_4$, R = La, Nd or Pr are fascinating. For instance $Nd_{1-x}Sr_{1+x}CoO_4$ ($0.25 \leq x \leq 0.6$) show spin-glass (SG) at 18K and Griffiths singularity around 210 K [11]. While the magnetic state of $La_{2-x}Sr_xCoO_4$ alters from AFM state to FM state when the doping level $x \geq 0.6$ [12]. Doping-dependent charge and superstructures in $Pr_{2-x}Ca_xCoO_4$ ($0.39 \leq x \leq 0.70$) and $La_{2-x}Sr_xCoO_4$ (x = 0.4, 0.61) were suggested [13]. It was found that the magnetic ordering of these systems is established at low temperature and has twice larger periodicity, indicating a dominant AFM correlation between the nearest Co^{2+} spins. The electrical behavior of $Nd_{1-x}Sr_{1+x}CoO_4$ system obeys Arrhenius law for x = 0.25, 0.33 and 0.60 due to hopping of small lattice polarons as in the case of manganites. A systematic increase of the resistivity with decreasing *A*-site rare earth ionic radius r^{+3} in cobaltates was reported earlier [14] implying that upon narrowing the band width, the mobility of e_g electrons is decreased. For $Pr_{1-x}Sr_{1+x}CoO_4$ samples, the resistivity and thermal activation energy decreases irregularly with increasing x [15].

Because the layered perovskite compounds exhibit interesting properties so that a good motivation is to through light on $Pr_{1-x}Sr_{1+x}CoO_4$ system, especially at 0.60, i.e. in the Sr rich side. Through the publications [15,16] there is no details about the physical properties of this system

at higher content of Sr samples. Therefore, two major issues were addressed in this article: first is to establish the crystal structure of $Pr_{0.4}Sr_{1.6}CoO_4$ sample with respect to $PrSrCoO_4$ one. Second, is to understand the evolution of the electric and magnetic properties with the crystal structure of these compounds. The results show that the temperature dependence of resistivity of $Pr_{0.4}Sr_{1.6}CoO_4$ is still semiconductor as in the case of $Nd_{0.4}Sr_{1.6}CoO_4$ [11]. Finally, Comparison with similar compounds of the same *x* is also discussed

2. EXPERIMENTAL DETAILS

The polycrystalline $Pr_{1-x}Sr_{1+x}CoO_4$ samples (0 and 0.6) were prepared by the solid state method. Stoichiometric mixtures of Pr_6O_{11} (4N, MTI), $SrCO_3$ (5N, cerac) and Co_3O_4 (4N, Aldrich) were well ground and palletized. Then the specimens were calcined at 1000 °C and sintered in oxygen at 1050 - 1150 °C for 48 h with intermediate grindings. The sintered samples were annealed in oxygen at 1200 °C for 48 h. These pellets were further annealed at lower temperature (550 - 600 °C) for 24 h in oxygen overpressure in order to achieve the high oxidation state close to 3. Both phase analysis and lattice parameters at room temperature were determined using an x-ray diffractometer Bruker D8, Germany with Cu K_α radiation (λ = 1.54056 Å). The x-ray diffraction (XRD) data were collected in $20° \le 2\theta \le 90°$, with 0.02° steps and 19 second acquisition times per step.

Electrical resistivity-temperature dependence, $\rho(T)$, curves were measured both on cooling and on heating by the standard dc four-probe method using a CCR type refrigerator. DC magnetization measurements were performed in a SQUID magnetometer (Quantum Design MPMS-5S). Magnetization temperature curves were measured in zero-field- cooled (ZFC) mode with an applied magnetic field (H) of 0.20 kOe and 5.0 kOe. The magnetization-applied field, M(H), curves were measured within $H = \pm 60$ kOe at 5 K.

3. RESULTS AND DISCUSSION

3.1. X-ray Diffraction

Polycrystalline $PrSrCoO_4$ and $Pr_{0.4}Sr_{1.6}CoO_4$ were characterized by conventional powder x-ray diffraction at room temperature employing Cu-K_α radiation. The investigated samples crystallize in the K_2NiF_4-type structure [15]. The crystal structure is described by space group I4/mmm with Pr/Sr ions at the Wyckhoff position 4*e* (0, 0, z) (z ≈ 0.35), Co ions at the 2*a* site (0, 0, 0) and oxygen ions at the 4*c* site (1/2, 0, 0) and the 4e site (0, 0, z) (z ≈ 0.16), respectively. The data were analyzed by standard Rietveld refinement employing the FULLPROF program suite [17]. The diffraction patterns showed single phase material for the investigated compounds. In particular, no indications of spurious perovskite-related phases could be detected. **Figure 1** shows representative diffractograms and the corresponding refinements of both $PrSrCoO_4$ and $Pr_{0.4}Sr_{1.6}CoO_4$ samples. The Rietveld refinements included the following fit parameters: overall scale factor, zero point shift, peak shape, isotropic temperature factors, 3 Cagliotti resolution parameters, the lattice constants *a* and *c*, the atomic positional parameters z(Pr/Sr) and z(O) of Pr/Sr and oxygen ions, respectively. Good agreement between observed and calculated intensities is achieved as reflected in the reliability factors. The structural properties of both samples are summarized in **Table 1**. The results show good agreement with values published in the literature [15]. The unit cell volume increases roughly with introducing more Sr as shown in **Table 1**. Interestingly, this change of the unit cell volume is predominantly originating by an increase of the tetragonal lattice constant *c*, whereas the lattice constant *a* within the equatorial plane remains almost constant. This behavior is similar to the results found for the La, Nd and Gd similar compounds [18] and a previous study [15] on $Pr_{1-x}Sr_{1+x}CoO_4$. It emphasizes the quasi two-dimensional character of the K_2NiF_4-type structure representing the $n = 1$ end member of the Ruddlesden-Popper phases. The change of the unit cell volume with Sr substitution is governed by two competing effects. The substitution of Pr^{3+} (ionic radius for nine-fold coordination is $r(Pr^{3+}) = 1.179$ Å) by Sr^{2+} ($r(Sr^{2+}) = 1.31$ Å) leads to a lattice expansion. On the other hand, charge neutrality implies oxidation of Co^{3+} (ionic radius for high spin state in six-fold coordination is $r(Co^{3+}) = 0.545$ Å) to Co^{4+} ($r(Co^{4+}) = 0.53$ Å). Obviously, the substitution of Pr by Sr is the dominating effect. In addition, the refinements also allow a determination of the bond length listed in **Table 1**. The ratio of the Co-oxygen bonds (apical bond length over equatorial bond length) reveal the distortion of the CoO_6 octahedra. This behavior is directly reflected in the z-coordinate of oxygen. In $Pr_{0.4}Sr_{1.6}CoO_4$, both the z-coordinate of oxygen, as well as the distortion reveal a strong increase. This behavior is in agreement with that found in previous study [15].

3.2. Electric Properties

The electrical resistivity as a function of temperature of both compounds represents in **Figure 2(a)**. The resistivity shows insulating behavior ($d\rho/dT<0$) consistent with previous reports [16] and homologue compounds $La_{1-x}S_{1+x}CoO_4$, as in [19]. The variation of ρ versus *T* follows Arrhenius law:

$$\rho = \rho_0 \exp(E/kT) \qquad (1)$$

where ρ_0 material constant, *k* Boltzmann's constant and *E* the activation energy. The inset of **Figure 2(b)** shows the linear fitting of the resistivity of $PrSrCoO_4$ against $1/T$, which yields the values of *E* as listed in **Table 2**. Although the resistivity of $Pr_{0.4}Sr_{1.6}CoO_4$ is smaller than that of $PrSrCoO_4$, the first compound is still semiconductor. As seen in **Figure 2(b)**, the behavior of ρ with $T^{-1/3}$ for $Pr_{0.4}Sr_{1.6}CoO_4$ obeys two-

dimensional variable range hopping (2D-VRH) [20] within the temperature range (97-300K) consistent with that reported for $Nd_{0.4}Sr_{1.6}CoO_4$, as in [11] and $Pr_{0.5}Sr_{1.5}CoO_4$, as in [16]. Based on 2D-VRH, the temperature dependent reistivity $\rho(T)$ of $Pr_{0.4}Sr_{1.6}CoO_4$ follows the relation:

$$\rho = \rho_0 \exp(T_0 / T)^{1/3} \qquad (2)$$

where T_0 is the variable range hopping parameter described by Mott and Davis [21]. The fitting of the rsistivity data of $Pr_{0.4}Sr_{1.6}CoO_4$ sample according to **Eq.2** gives the two parameters T_0 = 5.77 x 10^5 K and ρ_0 = 6.75 x10^{-4} (Ω cm).

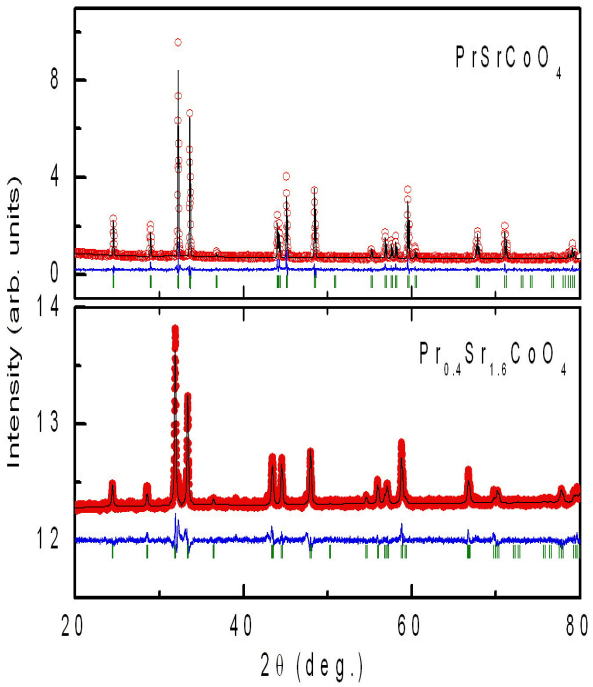

Figure 1: X-ray diffraction patterns of $PrSrCoO_4$ and $Pr_{0.4}Sr_{1.6}CoO_4$. Shown are observed intensities (open red circles), calculated intensities (full black line), their difference (blue line below) and the position of the calculated reflections (green vertical bars).

3.3. Magnetic Properties

Figure 3(a) depicts the zero field-cooled (ZFC) magnetic susceptibility, χ, at 0.20 and 5.0 kOe versus temperature for $Pr_{0.4}Sr_{1.6}CoO_4$ compound. While the sample the parent sample $PrSrCoO_4$ exhibits Curie-Weiss paramagnetic-like as shown in the inset of the upper frame of this figure, χ(T) of $Pr_{0.4}Sr_{1.6}CoO_4$ increases slightly with decreasing temperatures until the appearance of a pronounced peak. The increase of χ with increasing Sr content is due to the change of the ground state of $PrSrCoO_4$ of low spin state (LS) to the intermediate spin state (IS). Similar behavior was observed for $La_{2-x}Sr_xCoO_4$ system [22]. Moreover, the distortion of the tetragonal Jahn-Teller of CoO_6 octahedron in the K_2NiF_4-type structure plays a dominant role in stabilizing the IS configuration. Both height and position of such peak changes with the applied magnetic field. Another transition of this sample can also be seen around 160K. The first transition can be ascribed to a Griffiths phase (T_G) for $T_M < T < T_G$ with T_M denoting

Table 1. Structural parameters and bond lengths of $PrSrCoO_4$ and $Pr_{0.4}Sr_{1.6}CoO_4$ as resulting from the Rietveld refinements of the x-ray powder diffraction measurements. Space group is I 4/mmm with Pr/Sr ions at the 4(e) site with fractional coordinates (0, 0, z), Co ions at 2(a) sites with coordinates (0, 0, 0), oxygen O1 at the 4(c) site (0.5, 0, 0) and oxygen O2 at the 4(e) site (0, 0, z) are a given.

Sample	$PrSrCoO_4$	$Pr_{0.4}Sr_{1.6}CoO_4$
a (Å)	3.7774(1)	3.7801(4)
c (Å)	12.341(6)	12.433(2)
v (Å^3)	176.100(1)	177.663(7)
z (Pr/Sr)	0.3597(2)	0.3596(4)
z (O)	0.165(1)	0.178(3)
R_{Bragg} (%)	6.05	9.19
Co-O1 x2 (Å)	2.036(2)	2.21(2)
Co-O2 x4 (Å)	1.889(2)	1.890(2)
(Co–O1)/(Co-O2)	1.078	1.169
PrSr-O1 x1 (Å)	2.404(1)	2.26(3)
PrSr-O1 x4 (Å)	2.688(2)	2.714(4)
PrSr-O2 x4 (Å)	2.562(2)	2.573(3)

the temperature of the second corresponding anomaly in χ(T). The T_G refers to the formation of short-range ferromagnetic clusters with large spins in the paramagnetic (PM) matrix. T_M points to short-range ferromagnetic (FM) phase. The values of T_G and T_M for $Pr_{0.4}Sr_{1.6}CoO_4$ are 160K and 70K at 0.20 kOe, respectively. With increasing the applied magnetic field to 5.0 kOe, these magnetic transitions became broad and shifted towards lower temperatures (T_G = 140K , T_M = 58K). No spin glass phase (SG) was observed at low temperature for $PrSrCoO_4$ or $Pr_{0.4}Sr_{1.6}CoO_4$ as reported earlier for $Pr_{0.8}Sr_{1.2}CoO_4$, as in [16] and $Pr_{1-x}Sr_{1+x}MnO_4$ (x = 0.2, 0.40) [23].

Figure 3(b) represents the temperature dependence of the inverse magnetic susceptibility, χ^{-1}, for the two investigated samples. A Curie-Weiss (CW) behavior is observed over the entire temperature range for the sample $PrSrCoO_4$. Deviation from CW behavior is limited

to high temperatures T >160K for $Pr_{0.4}Sr_{1.6}CoO_4$. According to CW law, the effective paramagnetic moments, μ_{eff}, and CW temperature, T_θ were calculated and tabulated in **Table 2.** The effective magnetic moment μ_{eff} decreases with increasing Sr ions as reported earlier [22]. As seen in **Table 2**, T_θ is negative for $PrSrCoO_4$ and alters to positive for $Pr_{0.4}Sr_{1.6}CoO_4$. The change of sign of T_θ shows that the substitution of Pr^{3+} by Sr^{2+} ions changes the magnetic transitions from predominantly AFM to FM. Similar behavior was observed for the compounds $La_{1-x}S_{1+x}CoO_4$ with increasing the content of Sr ions [19]. To estimate the contribution of permanent magnetic moments at room temperatures, the CW susceptibility at room temperature was given [24,25]:

$$\chi^{CW}(300K) = \frac{C}{300K - T_\theta} \qquad (3)$$

where C is Curie constant. As shown in **Table 2**, $\chi^{CW}(300K)$ of $Pr_{0.4}Sr_{1.6}CoO_4$ is higher than that of $PrSrCoO_4$ due to increasing magnetic exchange**.**

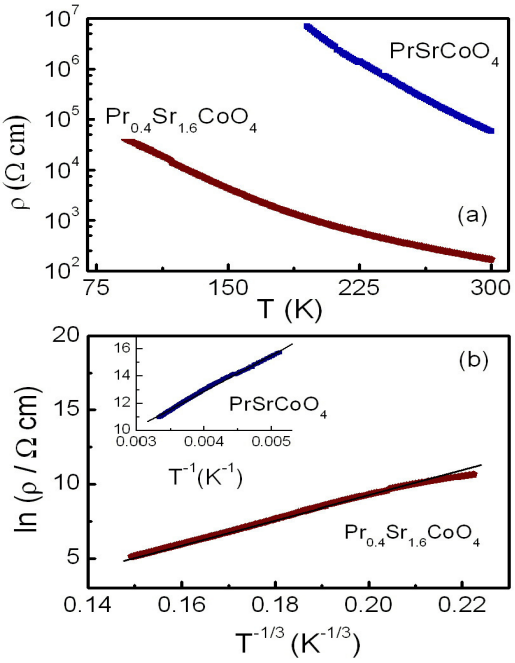

Figure 2: (a) Resistivity as a function of temperature of $PrSrCoO_4$ and $Pr_{0.4}Sr_{0.6}CoO_4$ samples (upper frame). (b) The variation of ln ρ against $T^{-1/3}$ for $Pr_{0.4}Sr_{1.6}CoO_4$. The inset in the lower frame displays the variation of ln ρ versus $1/T$ for $PrSrCoO_4$ sample. The solid lines display the linear fitting.

The isothermal magnetic behavior of the investigated samples at 5K with an applied magnetic field up to 60 kOe is shown in **Figure 4**. The paramagnetic behavior of $PrSrCoO_4$ is evidenced by negligible hysteresis although the magnetization, M(H), exhibits slight deviations from a strict linear behavior. On the other hand, the area of the hysteresis loop increases for $Pr_{0.4}Sr_{1.6}CoO_4$ but there is no evidence for fully developed FM phase.

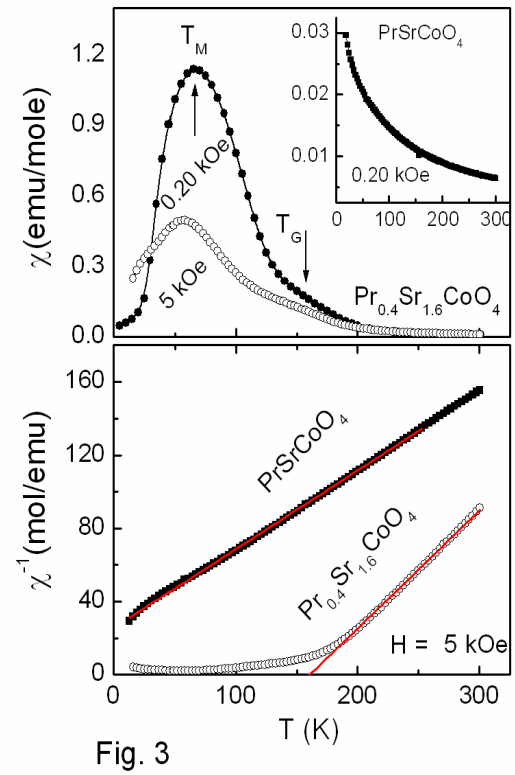

Figure 3: (a) The upper frame represents the zero-field cooled susceptibility, χ(T), of $Pr_{0.4}Sr_{1.6}CoO_4$ at H = 0.20 and 5.0 kOe. The corresponding magnetic transitions are indicated by arrows. The inset in the upper frame shows zero-field cooled susceptibility χ(T) of $PrSrCoO_4$ at 0.20 kOe applied field. (b) The lower frame depicts the temperature dependent of the inverse susceptibility $\chi^{-1}(T)$ for both investigated samples at 5 kOe. The solid lines represent the fitting according to Curie-Weiss (CW) law.

The maximum magnetization M_{max}(5K), remnant magnetization (M_r) and coercive field (H_{co}) were given for both samples in **Table 2**. Compared to previous reports on similar compounds with different Sr content [16], there is a good agreement with our results. On contrast, the homologue compounds $La_{0.5}Sr_{1.5}CoO_4$ shows ferromagnetic phase because partial saturation magnetization (1.5μ_B) at 2K was achieved [19]. The absence of ferromagnetism in $Pr_{1-x}Sr_{1+x}CoO_4$ compared to $La_{1-x}Sr_{1+x}CoO_4$ can be explained in terms of ionic radius of A-site (r_A) and tolerance factor (t):

$$t = \frac{r_A + r_O}{\sqrt{2}\,(r_B + r_O)} \qquad (4)$$

where r_B is the mean ionic radius of Co^{4+} and Co^{3+} ions and r_O is the ionic radius of O^{2-} ion. In the first system, r_A represents the average ionic radius of both Pr^{3+} and Sr^{3+} ions. Decreasing the values of t than one indicates an increasing of the buckling of the octahedra and then no complete FM phase is observed.. On contrast, r_A of the *A*-site in $La_{1-x}Sr_{1+x}CoO_4$ is larger than that of $Pr_{1-x}Sr_{1+x}CoO_4$ and $t>1$ so that FM was found for the first system.

Table 2. Magnetic properties of $PrSrCoO_4$ and $Pr_{0.4}Sr_{1.6}CoO_4$ compounds. The parameters were obtained by fitting $\chi^{-1}(T)$ data using Curie-Weiss (CW) law at 5 kOe applied field as shown in **Figure 4(b)**. The effective magnetic moment (μ_{eff}) , maximum magnetization at 5K ($M_{max,5K}$) and calculated CW magnetic susceptibility, χ^{CW} (300 K) in emu/mol K, coercive field (H_{co}) and remnant magnetization (M_r), the resistivity at room temperature, ρ_{300K} and activation energy , E, of $PrSrCoO_4$ are given.

sample	$PrSrCoO_4$	$Pr_{0.4}Sr_{1.6}CoO_4$
T_θ (K)	-59.65 ± 0.63	160.79 ± 0.48
μ_{eff}(μ_B /ion)	4.31 ± 0.22	3.52 ± 0.25
χ^{CW} (300K) x10^{-2}	0.65 ± 0.002	1.11 ± 0.005
$M_{max,5K}$ (μ_B)	0.19	0.81
H_{co} (kOe)	2.0	2.0
M_r (μ_B)	0.008	0.306
ρ_{300K} (Ω cm)	57673	168
E (meV)	228.8±1.436	-

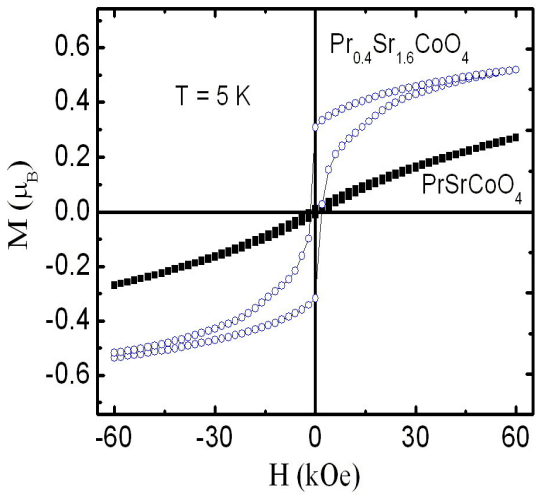

Figure 4: Magnetization hysteresis of $PrSrCoO_4$ and $Pr_{0.4}Sr_{0.6}CoO_4$ versus applied field (H) at 5 K**.**

4. CONCLUSIONS

The structural, transport and magnetic properties of $PrSrCoO_4$ and $Pr_{0.4}Sr_{1.6}CoO_4$ have been investigated. The Rietveld refinements of x-ray powder diffraction (XRD) patterns at room temperature indicate that both samples crystallize in K_2NiF_4-type structure with group symmetry I4/mmm. The lattice parameter *c* and unit cell volume of $Pr_{0.4}Sr_{1.6}CoO_4$ are higher than those of $PrSrCoO_4$ while the lattice constant *a* is almost the same. The electric measurement shows that $PrSrCoO_4$ is thermally activated within the studied range of temperature but the resistivity of $Pr_{0.4}Sr_{1.6}CoO_4$ obeys the two-dimensional variable rang hopping model (2D-VRH) within the range 97-300K of temperature. While the sample $PrSrCoO_4$ shows CW paramagnetic behavior in the studied range of temperature, $Pr_{0.4}Sr_{1.6}CoO_4$ undergoes two transitions: one due to Griffiths phase and second due to short range FM. Both transitions became broad and shifted toward low temperature with increasing applied magnetic field. No magnetic saturation was observed for the investigated samples at 5K and applied field up to 60 kOe. There is a strong relation between the structure and the physical properties of these compounds. It is expected that the expansion of the cell volume by increasing Sr content, influences the magnetic properties of this system. A neutron powder diffraction would be useful study to give more details about the magnetic structure of these samples.

5. ACKNOWLEDGEMENTS

The author would like to thank Prof. Dr. A. Krimmel for his help to analyze the x-ray diffraction, Prof. Dr. Bog. G. Kim for using some of his lab facilities and Dr. Somyia El-Sayed for her support during the performance of this work.

REFERENCES

[1] F. C. Chou, J. H. Cho, and Y. S. Lee, Phys. Rev. B **70**, 144526 (2004).

[2] S. Roy, I. S. Dubenko, M. Khan, E. M. Candon, and N. Ali, Phys. Rev. B **71**, 024419 (2005).

[3] R. Mahendiran and P. Schiffer, Phys. Rev. B **68**, 024427 (2003).

[4] R. H. E. van Doorn and A. J. Burggraaf, Solid State Ionics, **128**, 65 (2000).

[5] V. V. Kharton, A. A. Yaremchenko, A. V. Kovalevsky, A. P. Viskup, E. N. Naumovich, and P. F. Kerko, J. Membr. Sci. **163**, 307 (1999).

[6] G. H. Jonker and J. H. van Santen, Physica **19**, 120 (1953).

[7] V. G. Bhide, D. S. Rajoria, C. N. R. Rao, G. Rama Rao, and V. G. Jadhao, Phys. Rev. B **12**, 2832 (1975).

[8] P. Ganduly and C. N. R. Rao, in Metallic and Non-metallic State of Matter, edited by P. P. Edwards and C. N. R. Rao, Taylor & Francis, London, (1985).

[9] M. A. Senaris-Rodriguez and J. B. Goodenough, J. Solid State Chem. **118**, 323 (1995).

[10] K. Knížek, P. Novák, and Z. Jirák Phys. Rev. B **71**, 054420 (2005).

[11] S. Huang, K. Ruan, Z. Lv, L. Zhuang, P. Wei, H. Wu, M. Li, J. Zhang, Y. Chai, H. Yang, L. Cao, and X. Li, Phys. Rev. B **73**, 094431 (2006).

[12] Y. Furukawa, S. Wada, and Y. Yamada, J. Phys. Soc. Japan **62**, 1127 (1993).

[13] N. Sakiyama, I. A. Zaliznyak, S.-H. Lee, Y. Mitsui, and H. Yoshizawa, Phys. Rev. B **78,** 180406(R) (2008).

[14] R. Ang, Y. P. Sun, X. Luo, C. Y. Hao and W. H. Song, J. Phys. D: Appl. Phys. **41**, 045404 (2008).

[15] M. Li, S. L. Huang, Z. M. Lv, J. L. Zhang, H. Y. Wu, X. M. Wang, Z. Q. Pang and K. Q. Ruan, Mod. Phys. Lett. B **22**, 32, 3195 (2008).

[16] S. L. Huang, Z. C. Fan, J. B. Yi, B. C. Zhao, Y. Wu, K. Q. Ruan, M. Li, J. Ding and L. Wang, J. Phys. Condens. Matter **20,** 395213 (2008).

[17] J. Rodriguez-Carvajal, Physica B **192**, 55 (1993).

[18] M. Sánchez-Andújar and M. A. Seňaris-Rodŕiguez, Solid State Sciences **6**, 1, 21 (2004).

[19] Y. Shimada, S. Miyasaka, R. Kumai and Y. Tokura, Phys. Rev. **B** 73, 134424 (2006).

[20] B. I. Shklovskii and A. L. Efros: Electronic Properties of Doped Semiconductors, Springer Series in Solid State Sciences, Vol. 45 (Springer-Verlag), Berlin, Germany (1984).

[21] N. F. Mott and E.A. Davies: Electronic Processes in Noncrystalline Materials, Oxford University Press, Oxford, (1979).

[22] Y. Moritomo, K. Higashi, K. Matsuda, and A. Nakamura, Phys. Rev. B **55**, R14725–R14728 (1997)

[23] Y. Moritomo, Y. Tomioka, A. Asamitsu, Y. Tokura and Y. Matsui, Phys. Rev. B **51**, 3297 (1995).

[24] A. Hassen, A. I. Ali, B. J. Kim and Y. S. Wu, S. H. Park and Bog G. Kim, J. Appl. Phys. **102**, 123905 (2007)

[25] H. Hohl, A. P. Ramirez, T. T. M. Palstra and E. Bucher: J. Alloys Comp.**248**, 70 (1997).